Eur. Phys. J. B **44**, 21–32 (2005)
DOI: 10.1140/epjb/e2005-00095-5

THE EUROPEAN PHYSICAL JOURNAL B

A self-consistent TB-LMTO-augmented space recursion method for disordered binary alloys

A. Chakrabarti[1] and A. Mookerjee[2,a]

[1] Ramakrishna Mission Vivekananda Centenary College, Rahara, West Bengal, India
[2] S.N. Bose National Centre for Basic Sciences, JD Block, Sector III, Salt Lake, Kolkata 700098, India

Received 3 December 2004
Published online 16 April 2005 –

Abstract. We developed a complete self-consistent TB-LMTO-Augmented space recursion (ASR) method for calculating configurational average properties of substitutionally disordered binary alloys. We applied our method to fcc based Cu-Ni, Ag-Pd for different concentrations of constituent elements and body-centered cubic based ferromagnetic Fe-V (50−50) alloy. For this systems we investigated the convergence of total energy and l-dependent potential parameters, charges, magnetic moment, energy moments of density of states with the number of iterations. Our results show good agreement with the existing calculations and also with the experimental results where it is available. The Madelung energy correction due to the charge transfer has also been included by the method developed by Ruban et al.

PACS. 71.20.-b Electron density of states and band structure of crystalline solids – 71.23.-k Electronic structure of disordered solids

1 Introduction

The study of electronic structure of disordered alloys is of great scientific and technological importance. Theoretical approaches have achieved considerable success through the development of mean-field approximations, the most successful of which is the coherent potential approximation (CPA) [1]. Other techniques include super-cell approaches, attempted generalizations of the CPA and an alternative order-N Green's function technique [2]. The former is based on the self-consistent determination of a uniform medium to represent the substitutional alloy. The corresponding effective Hamiltonian is lattice transitionally symmetric and its Green function is a good approximation of the configurational averaged Green function. Of the later, the super-cell method is based on the study of different selected ordered structures at various concentrations. In these calculations a large unit cell is constructed which contains different possible configurations and is repeated to generate the entire lattice. The result of such a method contains the artifact of imposed lattice symmetry, which is OK provided we concentrate on the local properties at the centre of the super-cell whose size is rather large. There is no straight-forward rule for constructing a super-cell and in realistic calculations it becomes computationally expensive. A large number of generalizations of the CPA are beset with analytical difficulties and their effective medium are often not translationally symmetric. The only really successful generalization with analytic and translational properties is the traveling cluster approximation of Leath et al. [3].

The method chosen by us is a marriage between the augmented space theorem, proposed by one of us [4,5] (AST) and the recursion method [6] carried out in a minimal basis set of the tight-binding linear muffin-tin orbitals method (TB-LMTO) [7–9] in which the Hamiltonian is sparse. The AST states that the configuration average of a well behaved function of a set of random variables is a particular matrix element of the operator obtained by replacing the random variables in the function by the corresponding operators, whose spectral densities are the probability densities of the random variables. The underlying space in which the operator is defined is the space of all possible *configurations* of the random variables. For example, if the set of random variables have binary distributions, then this configuration space is isomorphic to the configuration space of a set of Ising spin-half objects. The theorem is *exact* and approximations are introduced only in the calculation of the matrix element. The recursion method with a terminator approximation allows us to take into account effects of random environments of a site. The size of this environment depends upon the number of recursion steps we can carry out *exactly* and the far environment is approximated by the terminator.

We shall present here a development of a code which will seamlessly join with the Stuttgart TB-LMTO code for

[a] e-mail: abhijit@bose.res.in

ordered materials to provide a self-consistent package for the study of the electronic structure of random binary alloys. It will allow us to go beyond the usual single-site CPA and include effects like short-ranged order [10,11], random clustering [12] and local lattice distortion due to size mismatch between the constituents [13]. Our code can also be used to study alloy systems which are non-stoichiometric and are only partially disordered [14] (for example only one sub-lattice is disordered).

As an application of our codes we shall study face-centered cubic based, paramagnetic AgPd and CuNi alloys for various compositions and body-centered cubic based, ferromagnetic 50−50 FeV. We shall calculate the atom-projected and total density of states (DOS), total energy and local magnetic moments on constituent atoms. We have also analyzed the charge redistribution among different orbitals in different constituents due to alloying. This helps us in understanding the magnetic moment contributions from m-resolved states of Fe and V in FeV. In addition to this we have studied in detail the convergence of the energy, moments, Fermi energy, potential parameters as a function of number of iterations. We have also studied the orbital resolved energy spectrum for the alloy constituents and the intra and inter atomic orbital hybridization.

2 The TB-LMTO-ASR code structure

The TB-LMTO-ASR code consists of five modules, as shown in Figure 1. Let us describe each of these modules in some detail.

Module A: Inputs and Structure The input data are provided in two control files 'CTRLA' and 'CTRLB'. These files are prepared for each constituent atom using the initialization programmes of the standard TB-LMTO package. However, the Wigner-Seitz radius for each constituent is replaced by the radius averaged with concentration weights:

$$r_{WS} = x_A\ r_A\ +\ x_B\ r_B.$$

These radii and the symmetries provided are checked by the subroutine 'chksym' provided by the TB-LMTO package. The subsequent subroutine 'strrs' calculates the structure matrices in the most tight-binding representation for the alloy lattice constant parameter.

The control files have additional informations as compared with the standard TB-LMTO package: for example, the concentration of the constituents, short-ranged order parameter for cases where there is short-ranged order, a flag which tells the subsequent program 'strrs' to calculate different structure matrices corresponding to local lattice distortion due to size mismatch (if it is required), concentrations of the constituents in different sub-lattices for partial ordering.

In addition, the control files also carry the formation required for the recursion programme: for example, the number of recursion steps to be taken, the number and position of the 'seed' energies and the type of terminator to be used.

Module B: Calculations within a single atomic sphere This module is taken directly from the Stuttgart TB-LMTO programme. It calculates the spherical charge density within an atomic sphere (AS). Then solving the Poisson equation obtains the Hartree part of the potential within that AS. It adds one of the chosen forms of the exchange-correlation potential and iterates the 'atomic' like calculations to self-consistency. After this it also calculates the one-atom contribution to the total energy and the muffin-tin zero for all different types of AS.

Module C: Potential parameters for different atoms This module is also taken directly from the Stuttgart TB-LMTO programme. It takes the input from Module B and calculates the potential parameters for different atoms sitting within different AS.

Module D: The ASR module This is the main contribution of this work. This module replaces the usual Bloch Theorem based band structure calculations via reciprocal space, by the augmented space method. Before we discuss the features of this module, we shall introduce the methodology first for the case where there is no short-ranged ordering, local lattice distortions and the disorder is homogeneous:

The Augmented space theorem coupled with the recursion method [15] form a basis for calculating local electronic structure properties of disordered alloys in real space [16,17]. As it is known that a localized tight-binding basis set is required for implementing recursion method, one can perform recursion based calculation in the frame work of the TB-LMTO. In our case we have used the second order TB-LMTO Hamiltonian:

$$\mathcal{H}^{(2)} = E_\nu + h - hoh \tag{1}$$

where,

$$\begin{aligned} h &= \sum_{RL} (C_{RL} - E_{\nu RL})\ \ \mathcal{P}_{RL} \\ &\quad + \sum_{RL} \sum_{R'L'} \Delta_{RL}^{1/2}\ S_{RL,R'L'}\ \Delta_{R'L'}^{1/2}\ \ \mathcal{T}_{RL,R'L'} \\ o &= \sum_{RL} o_{RL}\ \ \mathcal{P}_{RL} \end{aligned} \tag{2}$$

- C, o and Δ are potential parameters of the TB-LMTO method, these are diagonal matrices in the angular momentum indeces and they are derived self-consistently from a first principle theory. o^{-1} has the dimension of energy and is a measure of the energy window around E_ν around which the approximate Hamiltonian $\mathcal{H}^{(2)}$ is reliable. These 'local' random variables can be written in terms of local occupation numbers n_R for, say, the A atom, e.g. $C_{RL} = C_L^A\ n_R + C_L^B(1 - n_R)$.
- R denotes atomic position label associated with a TB-LMTO basis and $L = (\ell m m_s)$ is the composite angular momentum index.

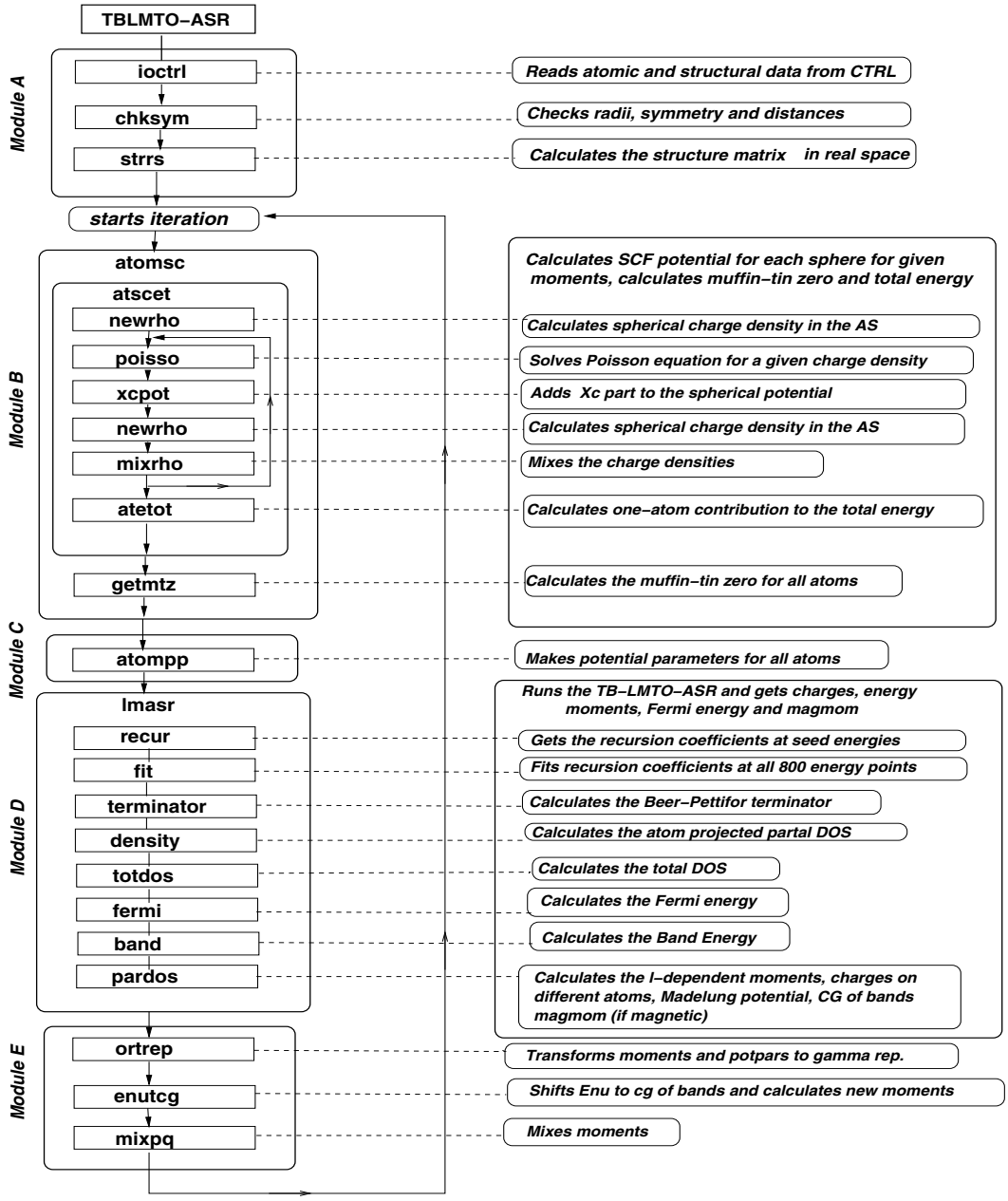

Fig. 1. The self-consistent TB-LMTO-ASR code structure.

– $S_{RL,R'L'}$ is called structure matrix, which depends only on the geometry of the underlying lattice. In the absence of local distortions, this is not random.
– $\mathcal{P}_{RL}$ and $\mathcal{T}_{RL,R'L'}$ are the projection and transfer operators in Hilbert space H spanned by tight-binding basis $\{|RL\rangle\}$:
$\mathcal{P}_{RL} = |RL\rangle\langle RL|$ and $\mathcal{T}_{RL,R'L'} = |RL\rangle\langle R'L'|$.

The Augmented space method associates with the random variables n_R, a set of operators M_R whose spectral densities are the probability densities of the variables. For a binary distribution of the n_R:

$$M_R = x_A \mathcal{P}_R^{\uparrow} + x_B \mathcal{P}_R^{\downarrow} + \sqrt{x_A\ x_B}\left\{\mathcal{T}_R^{\uparrow\downarrow} + \mathcal{T}_R^{\downarrow\uparrow}\right\}. \quad (3)$$

The Augmented space Hamiltonian is obtained by replacing the random variables by their corresponding operators. The theorem states then that a matrix element of the Green function of this Hamiltonian is the configuration averaged Green function. It was shown in [18] that we may write the expression for a partially averaged Green function (averaged over all sites except a particular R)

$$\langle G_{RL,RL}(E)\rangle = \left\langle 1\right| \left[E\hat{I}\ -\ \hat{H}\right]^{-1} \left|1\right\rangle$$
$$\text{where} \quad \hat{H} = \mathcal{P}_R\ \mathcal{H}^{(2)}\ \mathcal{P}_R + (I - \mathcal{P}_R)\ \tilde{H}\ (I - \mathcal{P}_R)$$
$$\text{and} \quad \tilde{H} = \hat{A} - \hat{B} - \hat{F} + \hat{S} - \left(\hat{J} + \hat{S}\right)\hat{o}\left(\hat{J} + \hat{S}\right). \quad (4)$$

If we label a 'configuration state' by the set of positions where a $\downarrow$ sit (called the cardinality sequence), then

$$|1\rangle = \left\{ \frac{A_L\left(\Delta^{-1/2}\right)}{\left[A_L(1/\Delta)\right]^{1/2}} \right\} \; |R, L, \otimes\{\emptyset\}\rangle + \ldots \left\{ \frac{F_L\left(\Delta^{-1/2}\right)}{\left[A_L(1/\Delta)\right]^{1/2}} \right\} \; |R, L, \otimes\{R\}\rangle \quad (5)$$

and,

$$\hat{A} = \sum_{R,L,} \left\{ \frac{A_L\left(C/\Delta\right)}{A_L\left(1/\Delta\right)} \right\} \mathcal{P}_{R,} \otimes \mathcal{P}_L \otimes \mathcal{I}$$

$$\hat{B} = \sum_{R,L,} \left\{ \frac{B_L\left(\left(E-C\right)/\Delta\right)}{A_L\left(1/\Delta\right)} \right\} \mathcal{P}_{R,} \otimes \mathcal{P}_L \otimes \mathcal{P}_R^{\downarrow}$$

$$\hat{F} = \sum_{R,L,} \left\{ \frac{F_L\left(\left(E-C\right)/\Delta\right)}{A_L\left(1/\Delta\right)} \right\} \mathcal{P}_{R,} \otimes \mathcal{P}_L \otimes \left(\mathcal{T}_R^{\uparrow\downarrow} + \mathcal{T}_R^{\downarrow\uparrow} \right)$$

$$\hat{S} = \sum_{RL} \sum_{R'L'} \left\{ A_L\left(1/\Delta\right)^{-1/2} \right\} S_{RL,R'L'} \left\{ A_L\left(1/\Delta\right)^{-1/2} \right\} \ldots \mathcal{T}_{R,R'} \otimes \mathcal{T}_{LL'} \otimes \mathcal{I}$$

here, $\hat{J} = \hat{J}_A + \hat{J}_B + \hat{J}_F$ and $\hat{o} = \hat{o}_A + \hat{o}_B + \hat{o}_F$, where,

$$\hat{J}_A = \sum_{R,L,} \left\{ \frac{A_L\left(\left(C-E_\nu\right)/\Delta\right)}{A_L\left(1/\Delta\right)} \right\} \mathcal{P}_{R,} \otimes \mathcal{P}_L \otimes \mathcal{I}$$

$$\hat{J}_B = \sum_{R,L,} \left\{ \frac{B_L\left(\left(C-E_\nu\right)/\Delta\right)}{A_L\left(1/\Delta\right)} \right\} \mathcal{P}_{R,} \otimes \mathcal{P}_L \otimes \mathcal{P}_R^{\downarrow}$$

$$\hat{J}_F = \sum_{R,L,} \left\{ \frac{F_L\left(\left(C-E_\nu\right)/\Delta\right)}{A_L\left(1/\Delta\right)} \right\} \mathcal{P}_{R,} \otimes \mathcal{P}_L \otimes \left(\mathcal{T}_R^{\uparrow\downarrow} + \mathcal{T}_R^{\downarrow\uparrow} \right)$$

$$\hat{o}_A = \sum_{R,L,} \left\{ A_L\left(\tilde{o}\right) A_L\left(1/\Delta\right) \right\} \mathcal{P}_{R,} \otimes \mathcal{P}_L \otimes \mathcal{I}$$

$$\hat{o}_B = \sum_{R,L,} \left\{ B_L\left(\tilde{o}\right) A_L\left(1/\Delta\right) \right\} \mathcal{P}_{R,} \otimes \mathcal{P}_L \otimes \mathcal{P}_R^{\downarrow}$$

$$\hat{o}_F = \sum_{R,L,} \left\{ F_L\left(\tilde{o}\right) A_L\left(1/\Delta\right) \right\} \mathcal{P}_{R,} \otimes \mathcal{P}_L \left(\mathcal{T}_R^{\uparrow\downarrow} + \mathcal{T}_R^{\downarrow\uparrow} \right)$$

where,

$$A_L(Z) = x_A \; Z_L^A + x_B \; Z_L^B$$
$$B_L(Z) = \left(x_B - x_A\right) \; \left(Z_L^A - Z_L^B\right)$$
$$F_L(Z) = \sqrt{x_A x_B} \; \left(Z_L^A - Z_L^B\right)$$

Z is any single site parameter.

In order to couple with TB-LMTO the module does the following operations:

- The input are the initial potential parameters obtained from the Module C.
- Using the potential parameters and the input concentrations, we set up the effective 'Hamiltonian' (3) and the starting state (4). Note that the effective 'Hamiltonian' is energy dependent. We choose a set of *seed* energies $\{E_s\}$ across the expected spectrum and carry out a three term recursion to obtain the recursion coefficients at the seed energies:

$$|1\rangle = |RL\rangle \qquad |0\rangle = 0$$

for

$$n \geq 1 \quad |n+1\rangle = \hat{H}(E_s)|n\rangle - \alpha_n(E_s)|n\rangle - \beta_n^2(E_s)|n-1\rangle$$

$$\alpha_n(E_s) = \frac{\langle n|\hat{H}|n\rangle}{\langle n|n\rangle} \qquad \beta_n^2(E_s) = \frac{\langle n+1|n+1\rangle}{\langle n|n\rangle}.$$

Then,

$$\left\langle G_{RL,RL}^{A/B}(z) \right\rangle = \cfrac{1}{z - \alpha_1 - \cfrac{\beta_1^2}{E - \alpha_2 - \cfrac{\beta_2^2}{E - \alpha_3 - \ldots}}} \quad (6)$$

This operation is carried out by the subroutine 'recur' and the output is a set of coefficients $\{\alpha_n(E_s), \beta_n(E_s)\}$. This is input into a fitting programme 'fit', which, assuming that the variation of the coefficients is weak across the band spline fits the coefficients at 800 energy points across the spectrum.

- Using these coefficients up to a number n, we now construct the terminator of the continued fraction. We have the flexibility to use a square-root, a Luchini-Nex [19] or a Beer-Pettifor [20] terminator. Once the terminator is formed using the routine 'terminator' the partial density of states and the total density of states are obtained as follows:

$$n_L^{A/B} = -\frac{1}{\pi} \, \Im m \left\langle G_{RL,RL}^{A/B}\left(E + i0^+\right) \right\rangle$$

and

$$n(E) = \sum_L \; \left[x_A \; n_L^A(E) + x_B \; n_L^B(E) \right].$$

These are carried out by the subroutines 'density' and 'totdos'.

- The Fermi energy, band energy and the energy moments are calculated as follows:

$$\int_{-\infty}^{E_F} dE n(E) = x_A \; n_A + x_B \; n_B$$
$$\int_{-\infty}^{E_F} dE E \; n(E) = E_B$$
$$\int_{-\infty}^{E_F} dE (E - E_\nu)^k \; n_L(E) = \mu_L^k. \quad (7)$$

These are obtained within the routine 'pardos'. In addition the total charge in an atomic sphere is also calculated.

- If we wish to introduce short-range order through the Warren-Cowley parameter α, the expression for the

augmented space operator in (3) for the sites R' neighbouring the central site R becomes [10,11]:

$$\begin{aligned} M_{R'} = & x_A \mathcal{P}_R^{\uparrow} \otimes \mathcal{P}_{R'}^{\uparrow} + x_B \mathcal{P}_R^{\uparrow} \otimes \mathcal{P}_{R'}^{\downarrow} \\ & \ldots + \Big\{ (1-\alpha) x_A + \alpha x_B \Big\} \mathcal{P}_R^{\downarrow} \otimes \mathcal{P}_{R'}^{\uparrow} \\ & + \Big\{ \alpha x_A + (1-\alpha) x_B \Big\} \mathcal{P}_R^{\downarrow} \otimes \mathcal{P}_{R'}^{\downarrow} \ldots \\ & \ldots + \Big\{ B_1 \mathcal{P}_R^{\uparrow} + B_2 \mathcal{P}_R^{\downarrow} + B_3 \mathcal{P}_{R'}^{\uparrow} - B_3 \mathcal{P}_{R'}^{\downarrow} \\ & + B_4 \left(\mathcal{T}_R^{\uparrow\downarrow} + \mathcal{T}_R^{\downarrow\uparrow} \right) \Big\} \otimes \left(\mathcal{T}_{R'}^{\uparrow\downarrow} + \mathcal{T}_{R'}^{\downarrow\uparrow} \right) \end{aligned} \quad (8)$$

where

$$\begin{aligned} B_1 &= x_A \sqrt{(1-\alpha) x_B (x_A + \alpha x_B)} \\ &\quad + \ldots x_B \sqrt{(1-\alpha) x_A (x_B + \alpha x_A)} \\ B_2 &= x_B \sqrt{(1-\alpha) x_B (x_A + \alpha x_B)} \\ &\quad + \ldots x_A \sqrt{(1-\alpha) x_A (x_B + \alpha x_A)} \\ B_3 &= \alpha \sqrt{x_A x_B} \\ B_4 &= \sqrt{x_A x_B} \left(x_B \sqrt{(1-\alpha) x_B (x_A + \alpha x_B)} \ldots \right. \\ &\quad \left. \ldots - x_A \sqrt{(1-\alpha) x_A (x_B + \alpha x_A)} \right). \end{aligned}$$

– In case we wish to introduce local lattice distortion, then, for an end-point approximation, the expression for the structure matrix in (2) is replaced by [13]:

$$S^{BB}_{RL,R'L'} + (n_R + n_{R'}) S^{(1)}_{RL,R'L'} + n_R n_{R'} S^{(2)}_{RL,R'L'} \quad (9)$$

where

$$S^{(1)}_{RL,R'L'} = S^{BB}_{RL,R'L'} - S^{AB}_{RL,R'L'}$$

$$S^{(2)}_{RL,R'L'} = S^{AA}_{RL,R'L'} + S^{BB}_{RL,R'L'} - S^{AB}_{RL,R'L'} - S^{BA}_{RL,R'L'}.$$

Since the local distance between AA, BB and AB are different when there is a local lattice distortion, the three structure matrices are calculated separately.

– Finally, we estimate the Madelung potential and energy. Since the constituents atoms in an alloy are different, there should be charge transfer between them. On alloying neutral atomic spheres may become charged, as a result there will be a significant contribution of a Madelung energy. Although, evaluation of this Madelung energy is quite straightforward for ordered alloys, no completely satisfactory method for its calculation in disordered alloys. For a mean-field coherent potential approach, which is equivalent to an isomorphous model, Kudrnovský and Drchal [21] have suggested using different atomic radii for the constituents in such a way that average total volume is conserved and the overlap is below our threshold value (15%), we can make these spheres approximately neutral and therefore ignore the Madelung contributions. Not only is the procedure varying the ratio $r = R_A/R_B$ (R_a is the atomic sphere radii) very cumbersome, Ruban and Skriver [22] have shown that local environmental effects (beyond the CPA) destroys the strict charge-potential alignment, and hence the possibility of choosing electroneutral atomic spheres by a single ratio r. In this development we have chosen rather to follow the procedure of Ruban and Skriver [22] and define a one-electron potential:

$$V_i = -\frac{Q_i}{R_a}$$

where, $i = A$ or B (labels the constituents of the alloy), Q_i is the net charge of the alloy component i in its own atomic sphere of radius R_a and is a screening parameter, which we vary arbitrarily according to our needs without specifying its physical meaning. We note that $= -\infty$ corresponds to the electro-neutral case (Q_i=0), while $= 0$ to the limit where there is no response of the system to charge transfer effects. The Madelung energy is then given by:

$$E_{Madelung} = \frac{Q_i Q_j}{R_a}.$$

Note that in this approach we use a single averaged atomic radius $\langle R_a \rangle$ for both the components.

Thus the Module D has as outputs the following: The L-dependent energy moments in the most tight-binding representation, the charges in different atomic spheres, the Madelung potentials, the centre-of gravity of the bands and, if it is a magnetic calculation, then the magnetic moment associated with different atomic spheres.

Within this module we have kept an option which switches from the simple ASR-code to one (SRO-ASR) which includes the effect of short-ranged order [10,11]. We may also switch from the simple ASR-code to one in which the effects of size mismatch is taken into account within a end-point approximation [13]. These switches are additional switches available in the CTRL files.

Module E: Change of representation and mixing This last module changes the moments from the most tight-binding to the orthogonal representation, shifts the E_ν to the centre of the bands and mixes all output with their original in-out values using a linear mixing. At present only linear mixing has been used, as we found difficulties of convergence with non-linear mixing.

The procedure is iterated to the desired accuracy in the total energy, atomic sphere charges and (in case of magnetic alloys) also local magnetic moments. On convergence the output gives us the partial and total density of states, the Fermi energy, the total energy, the magnetic moments, charge and moment distributions within the atomic spheres and the converged potential parameters.

3 Some applications

3.1 The 50–50 FeV ferromagnetic binary alloy

The Figure 2 shows the Fe and V projected density of states for a 50−50 FeV body-centered cubic (bcc) alloy.

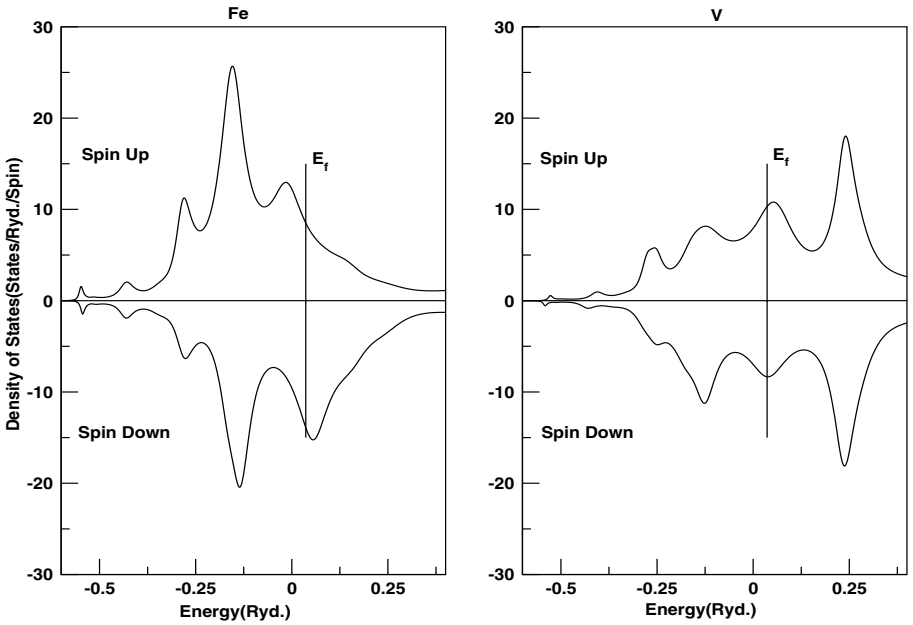

Fig. 2. The projected, spin resolved density of states on the Fe (left panel) and V (right panel) atoms in 50−50 bcc FeV.

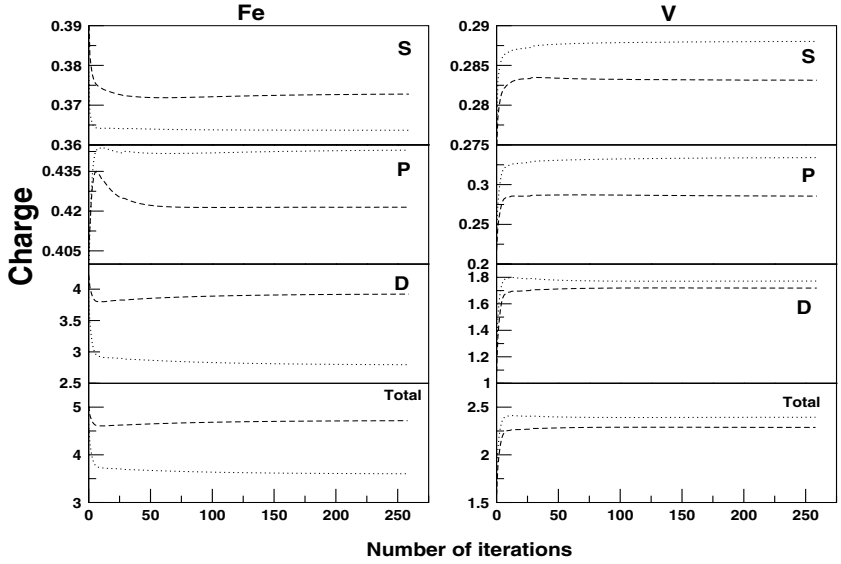

Fig. 3. The convergence of orbital and spin-resolved charges in Fe and V atomic spheres. Dashed curves indicate spin-up states and dotted ones the spin-down states.

The calculation was carried out within a local spin density approximation (LSDA), with the initial spin resolved charges given to be different for both Fe and V atomic spheres.

Figures 3 and 4 shows how the orbital projected charges and magnetic moments in the Fe and V atomic spheres converge with the number of iterations of the self-consistency cycle. We notice that although the convergence of the charges is rather fast, the moment convergence is comparatively slower. This has prompted us to put an additional convergence criterion for the magnetic moment in our Module E.

Decrease in saturation magnetization of Fe when it is alloyed with $3d$ elements like V has been observed experimentally. Here we analyze how this alloying affects the Fe and V projected density of states and the charge redistribution mechanism which results in suppression of Fe magnetic moment in the alloy. Table 1 shows the converged orbital projected charge and magnetic moment of Fe and V in a 50−50 FeV alloy. We observe charge transfer from V to Fe by an amount 0.31 as compared to the pure bulk Fe. But the spin up band in Fe in the alloy looses 0.41 amount of charge compared to bulk, whereas the minority band gains 0.72 amount of charge. If the excess charge from V went entirely to the minority band, then the magnetic moment would have been 1.94. However,it is the intratomic charge transfer from majority to minority band which further lowers the magnetic moment by

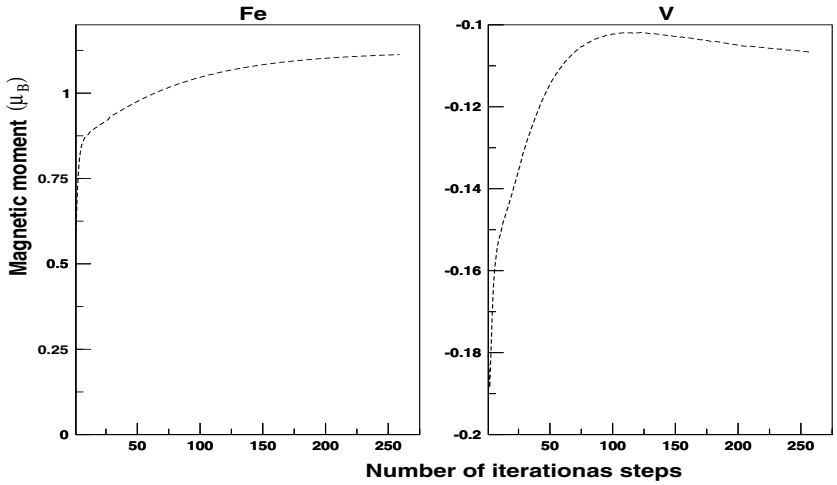

Fig. 4. Convergence of the Fe and V projected magnetic moments with iteration steps of the self-consistency cycle.

Table 1. The orbital resolved charges in Fe and V atomic spheres in FeV alloy. A comparison is shown for bulk pure Fe.

	Fe in 50−50 FeV alloy					
	s	p	t_{2g}	e_g	Total Charge	Net Magnetic moment of FeV
Spin up	0.37	0.42	2.34	1.58	4.72	
Spin down	0.36	0.44	1.88	0.92	3.60	1.12
	V in 50−50 FeV alloy					
Spin up	0.28	0.29	1.72		2.29	
Spin down	0.29	0.33	1.77		2.39	−0.11
	Pure Fe					
Spin up	0.32	0.37	2.56	1.88	5.12	
Spin down	0.33	0.42	1.50	0.63	2.88	2.25

0.82. The picture here is more interesting because though the majority band of FeV in the alloy has lost charge but its s and p sub-bands have gained compared to pure Fe. This interesting interplay between orbitals and the consequent charge transfer has been captured by our analysis. Our magnetic moment of Fe in FeV alloy matches well with experimental observations [23]. Previous theoretical calculations [24] were comparatively inaccurate.

3.2 Ag_xPd_{1-x} and Cu_xNi_{1-x} paramagnetic binary alloys

Next, we choose to study the two alloy systems AgPd and CuNi for the following reasons:

– Both alloys remain face-centered cubic solid solutions throughout the concentration range. There is very little size mismatch between the constituents in either system. The disorder is then dominated by the diagonal terms in the Hamiltonian.
– Both systems have been extensively studied earlier through the CPA formalism. We may therefore be able to compare our results with them. Moreover, for both systems the d-band centers of the constituents are well separated. In such alloys, particularly in the dilute regime, one expects environmental and cluster effects to be important. Our TB-LMTO-ASR should be able to capture this.
– Since in this work we have incorporated the charge transfer effect, and there exist controversy regarding the direction and nature of charge transfer in this alloys, we tried to shed light on this matter.

The general features are as follows:

– The structure in DOS mainly comes from the 4s-5d electron in Ag and Pd. For small concentration of Pd in Ag, the Pd impurity forms a level half-way between the top of host Ag d-band and Fermi energy. As the Pd concentration is increased the impurity band widens, while the Ag band loses its structure due to disorder scattering. On the other hand as Pd concentration goes beyond 50%, its shape approaches that of pure Pd and Ag forms a impurity level below the Pd d-band. This is clearly seen in Figure 5. The DOS agrees closely with the CPA results of Kudrnovský and Drchal [21] and earlier work of Saha, Dasgupta and Mookerjee [12].
The same feature has also been observed for CuNi system [25], as seen in Figure 6. It is also a split band type of alloy. For larger concentration of one constituent, the other forms a impurity band and the former approaches the shape of pure metal. This is characteristic of alloys whose constituents have well separated bands. All these features have been confirmed by earlier studies.

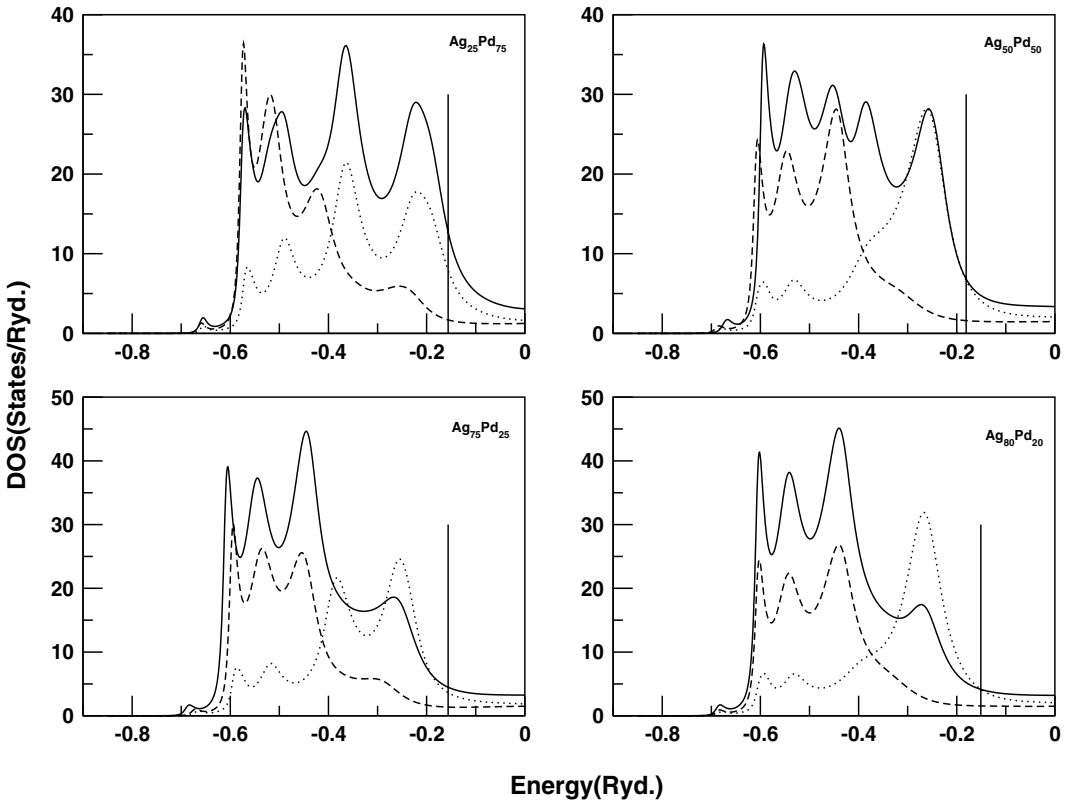

Fig. 5. Ag-projected DOS (dashed line), Pd-projected DOS (dotted line) and total DOS (full line) for different alloy concentrations shown in the figure for AgPd alloy.

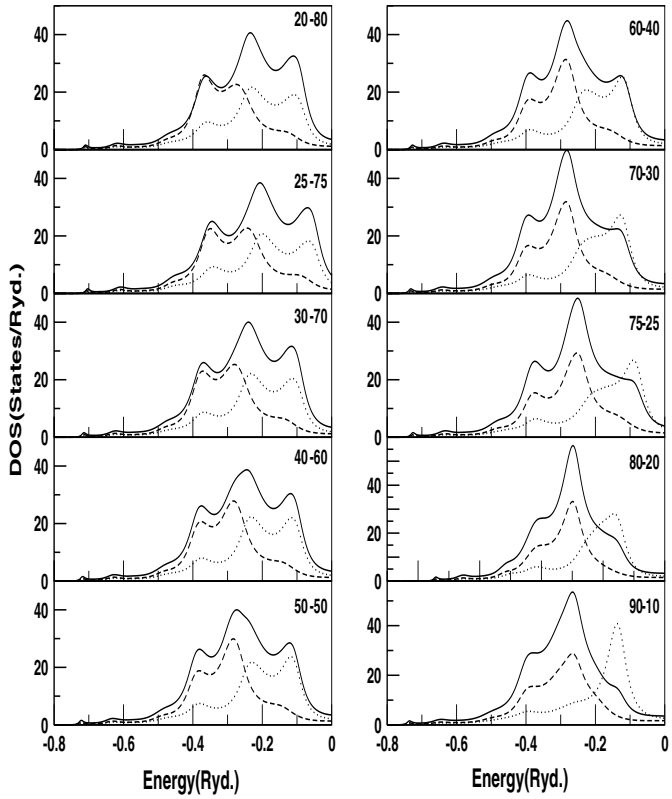

Fig. 6. Cu-projected DOS (dashed line), Ni-projected DOS (dotted line) and total DOS (full line) for various alloy concentrations shown in the figure for Cu-Ni alloys.

Table 2. Orbital resolved charges in the atomic spheres for (top) AgPd alloys and (bottom) CuNi alloys.

	Ag_x				Pd_{1-x}			
x	s	p	d	Total Charge	s	p	d	Total Charge
0.0					0.61	0.67	8.72	10.0
0.25	0.70	0.70	9.53	10.93	0.63	0.64	8.75	10.02
0.50	0.70	0.66	9.58	10.93	0.62	0.60	8.85	10.07
0.75	0.70	0.67	9.59	10.96	0.61	0.60	8.90	10.11
0.80	0.70	0.66	9.60	10.96	0.62	0.60	8.93	10.15
1.0	0.69	0.66	9.65	11.00				
	Cu_x				Ni_{1-x}			
x	s	p	d	Total Charge	s	p	d	Total Charge
0.0					0.65	0.76	8.60	10.00
0.20	0.74	0.80	9.44	10.98	0.68	0.74	8.59	10.00
0.25	0.73	0.82	9.42	10.98	0.68	0.76	8.58	10.01
0.30	0.74	0.80	9.44	10.98	0.68	0.74	8.60	10.01
0.40	0.74	0.80	9.46	10.98	0.67	0.73	8.61	10.02
0.50	0.73	0.79	9.46	10.98	0.67	0.72	8.63	10.02
0.60	0.73	0.78	9.47	10.98	0.67	0.72	8.64	10.03
0.75	0.73	0.78	9.46	10.98	0.66	0.73	8.66	10.06
0.9	0.73	0.76	9.50	10.99	0.66	0.70	8.72	10.08
1.0	0.70	0.75	9.56	11.0				

– Recently Coulthard and Sham [26] made a detailed experimental study of character and direction of charge transfer in AgPd alloy. According to their result, both Pd and Ag gain d- charge and lose non d-charge compared with pure metals. The result shows that the net charge transfer to be from Ag to Pd. Other experiments also support the fact that Pd site gains more d-charge with increasing Ag content. Here, we carried out detail orbital resolved study of charge transfer effect in AgPd alloy, for different concentration of constituents. Our result reveal that:

– Net charge transfer in this alloy is from Ag to Pd (Tab. 2), which is in agreement with electronegative arguments and also confirmed by previous experiments.

– The Pd site gains more d-type charge with increasing Ag concentration, as confirmed by the experiment. But the charge transfer character of non d-type charges is not simple. We observe that at 75% Pd concentration, Ag loses 0.04 amount of p-charge and 0.03 of s-charge from the value of pure Ag. For most concentrations there is negligible transfer from these orbitals.

– The Ag-site loses d-type charge with increase in Pd concentration, this observation is in contradiction to the experimental observation of Coulthard and Sham. But this is in support of the theoretical work done by Kokko et al. [27]. The character of non-d charges is not monotonic, but they are such that at each concentration the net charge transfer is from Ag to Pd.

– The same trend has also been observed for CuNi alloys [28], with the net charge transfer from Cu to Ni (Tab. 2). The Cu/Ni site loses/gains d-type charge with increase in Ni/Cu concentration. The non d-charges in this alloy are such that they maintain the direction of net charge transfer (Cu to Ni) through out the concentration range.

In Figure 7 and in Figure 8 we show the convergence of the orbital resolved charges in the Ag and Pd atomic spheres of AgPd(50−50) alloy and Cu and Ni atomic spheres in CuNi($20-80$) alloy respectively. It is important to note that the charges converge quite rapidly with self-consistency iterations. This is because objections have often been raised about the convergence and stability of the recursion method used as the basic tool for calculating these quantities. Figure 9 shows the convergence of the first two moments of the charge distribution for AgPd. The convergence is not monotonic, but nevertheless within our error bar for more than 100 iteration steps. Ordinary linear mixing has been used for both alloys.

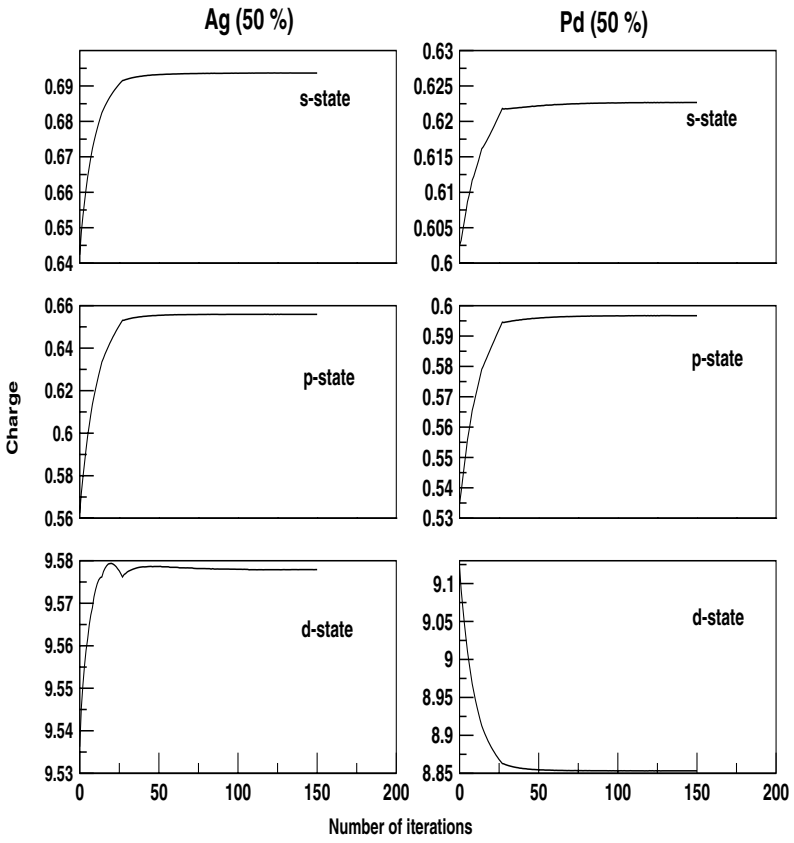

Fig. 7. Convergence of orbital resolved charge of Ag and Pd for AgPd (50−50) alloy.

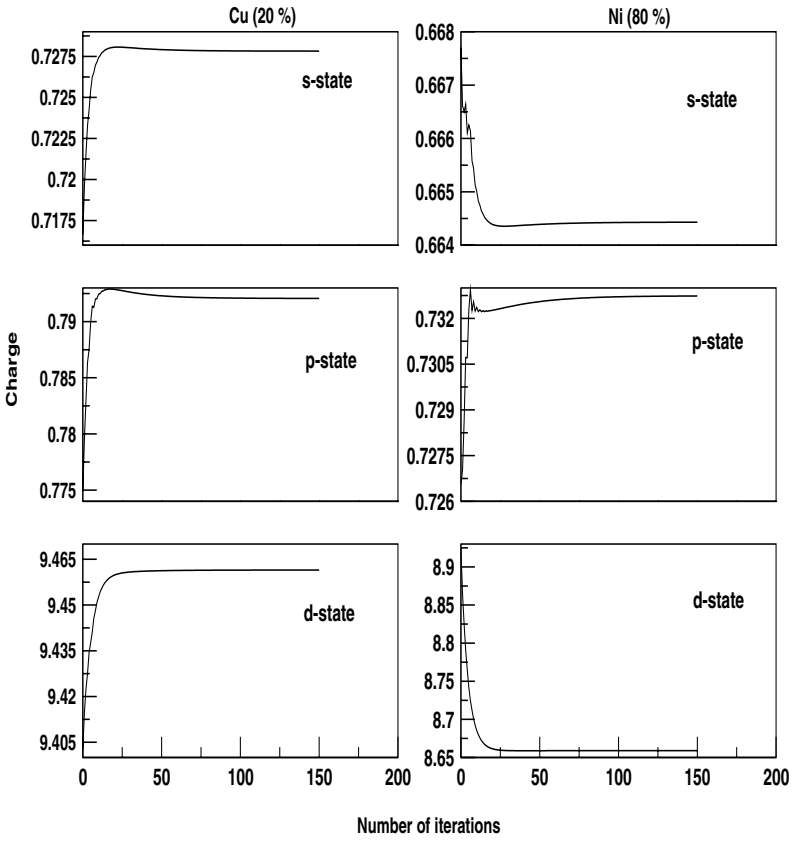

Fig. 8. Convergence of orbital resolved charge of Cu and Ni for CuNi(20 − 80) alloy.

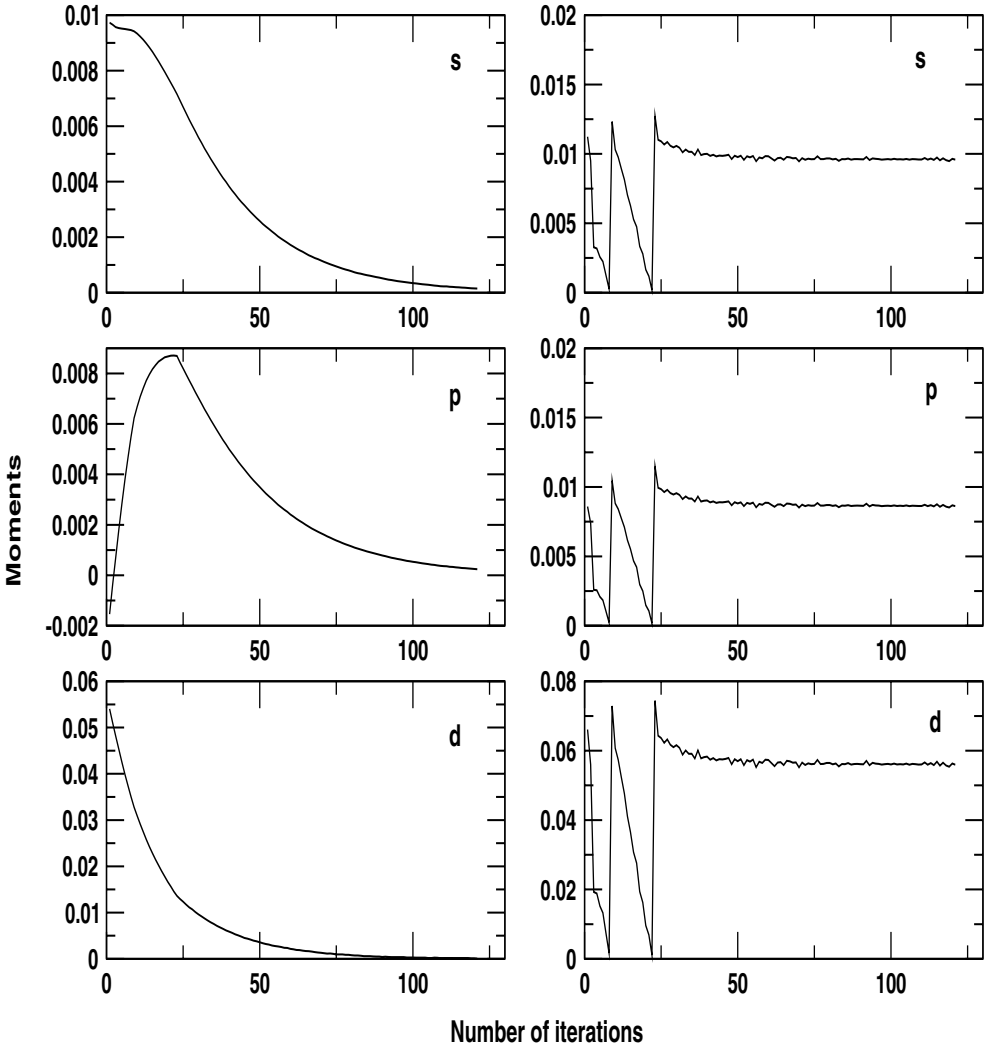

Fig. 9. Convergence of orbital resolved first moment (left panel) and second moment (right panel) for AgPd$(80-20)$ alloy.

One of us (AC) would like to thank Prof. O.K. Andersen, MPI, Stuttgart, Germany for hospitality during his stay in Stuttgart where a major part of this work was carried out. He would also like to acknowledge important discussions with Profs. O.K. Andersen and O. Jepsen during that time, and with Monodeep Chakrabarti of S.N. Bose National Centre, Kolkata. He also acknowledges infrastructural facilities of the S.N. Bose National Centre for Basic Science, Kolkata, India.

References

1. F.J. Pinski, B. Ginatempo, D.D. Johnson, J.B. Staunton, G.N. Stocks, B.I. Gyorffy, Phys. Rev. Lett. **66**, 766 (1991)
2. I.A. Abrikosov, A.M.N. Niklasson, S.I. Simal, B. Johansson, A.V. Ruban, H.L. Skriver, Phys. Rev. Lett. **76**, 4203 (1996)
3. T. Kaplan, P.L. Leath, L.J. Gray, H.W. Diehl, Phys. Rev. B **24**, 1872 (1981)
4. A. Mookerjee, J. Phys. C: Solid State Phys. **6**, L205 (1973)
5. A. Mookerjee, J. Phys. C: Solid State Phys. **6**, 1340 (1973)
6. R. Haydock, V. Heine, M.J. Kelly, J. Phys. C: Solid State Phys. **5**, 2845 (1972)
7. O.K. Andersen, *Computational Methods in Band Theory*, edited by P.M. Marcus, J.F. Janak, A.R. Williams (Plenum, New York, 1971), p. 178
8. O.K. Andersen, O. Jepsen, Phys. Rev. Lett. **53**, 2571 (1984)
9. O.K. Andersen, O. Jepsen, G. Krier *Lectures on Methods of Electronic Structure Calculations*, edited by V. Kumar, O.K. Andersen, A. Mookerjee (World Scientific, Singapore, 1994), p. 63
10. A. Mookerjee, R. Prasad Phys. Rev. B **48**, 17724 (1993)
11. T. Saha, I. Dasgupta, A. Mookerjee, Phys. Rev. B **50**, 13267 (1994)
12. I. Dasgupta, T. Saha, A. Mookerjee, J. Phys. C: Solid State Phys. **8**, 1979 (1996)
13. T. Saha, A. Mookerjee, J. Phys. C: Solid State Phys. **8**, 2915 (1996)

14. A. Chakrabarti, A. Mookerjee, J. Phys. C: Solid State Phys. **13**, 10149 (2001)
15. R. Haydock, J. Phys. C: Solid State Phys. **7**, 2120 (1972)
16. T. Saha, I. Dasgupta, A. Mookerjee, J. Phys. C: Solid State Phys. **6**, L245 (1994)
17. I. Dasgupta, T. Saha, A. Mookerjee, Phys. Rev. B **51**, 3413 (1995)
18. S. Ghosh, N. Das, A. Mookerjee, J. Phys. C: Solid State Phys. **9**, 10701 (1997)
19. M.U. Luchini, C.M.M. Nex, J. Phys. C: Solid State Phys. C **20**, 3125 (1987)
20. N. Beer, D.G. Pettifor, *The Electronic Structure Of Complex Systems*, edited by P. Phariseau, W.M. Temmerman, NATO ASI Series B **113**, 769 (1982)
21. J. Kudrnovský, V. Drchal, Phys. Rev. B **41**, 7515 (1990)
22. A.V. Ruban, H.L. Skriver, Phys. Rev. B **66**, 2402 (2003)
23. J.C. Krause, J. Schaf, M.I. da Costa, Jr., C. Paduani, Phys. Rev. B **61**, 6196 (2000)
24. I. Turek, V. Drchal, J. Kudrnovský, M. Sob, P. Weinberger, *Electronic Structure of Disordered Alloys, Surfaces and Interfaces* (Kluwer Academic Publishers, Boston, 1997) p. 227, Fig. 8.1
25. B.E.A. Gordon, W.E. Temmerman, B.L. Gyorffy J. Phys. C: Solid State Phys. **11**, 821 (1981)
26. I. Coulthard, T.K. Sham Phys. Rev. Lett. **77**, 4824 (1996)
27. K. Kokko, R. Laihia, M. Alatalo, P.T. Salo, M.P.J. Punkkinen, I.J. Vyrynen, W. Hergert, D. Kdderitzsch, Phys. Rev. B **60**, 4659 (1999)
28. H.H. Hseih, Y.K. Chang, W.F. Pong, J.Y. Pieh, P.K. Tseng, T.K. Sham, I. Coulthard, S.J. Naftel, J.F. Lee, S.C. Chung, K.L. Tsang Phys. Rev. B **57**, 15204 (1998)